

Data-driven regularization parameter selection in dynamic MRI

Matti Hanhela^{1*} Olli Gröhn² Mikko Kettunen²
Kati Niinimäki³ Marko Vauhkonen¹ Ville Kolehmainen¹

¹ Department of Applied Physics, University of Eastern Finland, 70211
Kuopio, Finland

² A.I. Virtanen Institute for Molecular Sciences, University of Eastern
Finland, 70211 Kuopio, Finland

³ Xray Division, Planmeca Oy, Asentajankatu 6, 00880 Helsinki, Finland

April 7, 2020

Submitted to Magnetic Resonance in Medicine

*matti.hanhela@uef.fi

Abstract

Purpose: In dynamic MRI, sufficient time resolution can often only be obtained using imaging protocols which produce undersampled data for each image in the time series. This has led to the popularity of compressed sensing (CS) based image reconstruction approaches. One of the main problems in the CS approaches is determining the regularization parameters, which control the balance between the data fidelity term and the spatial and temporal regularization terms.

Methods: A data-driven approach is proposed for the regularization parameter selection such that the reconstructions yield expected sparsity levels in the regularization domains. The expected sparsity levels are obtained from the measurement data for the temporal regularization and from a reference image for the spatial regularization. Two formulations are proposed. The first is a 2D search for a parameter pair which produces expected sparsity in both the temporal and spatial regularization domains. In the second approach, the sparsity-based parameter selection is split to two 1D searches using the S-curve method. The approaches are evaluated using simulated and experimental DCE-MRI data.

Results: In the simulated test case, both methods produce a parameter pair that is close to the optimal pair, and the reconstruction error is also close to minimum. In the experimental test case, the methods produce almost similar parameter selection, and the reconstructions are of high perceived quality.

Conclusion: Both approaches lead to a highly feasible selection of the temporal and spatial regularization parameters in both the simulated and experimental test cases while the second method is computationally more efficient.

Keywords— dynamic MRI, compressed sensing, regularization parameter, parameter selection, s-curve

1 Introduction

Dynamic magnetic resonance imaging is used to study hemodynamics, microvascular structure and function by contrast agent or stimulus related changes in a time series of MR images. High spatial and temporal resolution of the dynamic image series is often required for accurate analysis of the contrast agent or stimulus dynamics. In many cases, sufficient time resolution can only be obtained by utilizing an imaging protocol which produces undersampled data for each image in the time series. This, however, has the complication that reconstructing undersampled datasets with conventional MR image reconstruction methods, such as regridding [1], lead to noisy image series with poor spatial resolution.

Recently, the compressed sensing (CS) framework has led to significant advances in MRI with undersampled data. The theory of CS states that a target signal or image that is sparse in some basis, which is also incoherent with the measurement basis, can be perfectly reconstructed from undersampled data with a high probability [2–4]. Compressed sensing based approaches have been developed for numerous applications in both static and dynamic MRI, see for example the review [5].

Provided that the temporal resolution of the MR image series is high enough, one can expect high redundancy in the image series in the sense that the image intensity changes between successive image frames are small and occur only in some parts of the image domain. Therefore a compressed sensing approach based on the sparsity of the time derivative of the images is warranted.

The basic structure in the CS approaches to dynamic MRI is to reconstruct the whole time series of images simultaneously using an appropriate joint reconstruction formulation where a temporal regularization functional is employed for coupling the undersampled data across the time series of images. The most popular approach has been to use total variation (TV) regularization to promote sparsity of the spatial and temporal derivatives of the images, leading to a formulation [6, 7]

$$\hat{u} = \arg \min_u \{D(u, m) + \alpha \text{TV}_S(u) + \beta \text{TV}_T(u)\} \quad (1)$$

where $u = \{u^1, u^2, \dots, u^T\}$ denotes the time series of unknown images, $m = \{m^1, m^2, \dots, m^T\}$ is the MRI data time series, T is the number of time frames, D is the data fidelity term,

TV_S is the spatial total variation regularization functional, TV_T is the temporal TV regularization functional and α and β are the spatial and temporal regularization parameters, respectively.

The selection of the regularization parameters is crucial in terms of resulting image quality. Several classical parameter selection methods, such as the Morozov discrepancy principle or the L-curve method, exist, but these have been designed for the selection of a single regularization parameter and derived for a restricted class of problems. Thus, the parameters (α, β) are typically selected by subjective visual assessment of the reconstructions.

In this work, we propose a data-driven approach for the selection of the regularization parameters α and β in Eq. (1). The proposed idea is to select a parameter pair which produces an *a priori* expected level of sparsity in both the domain of the spatial TV regularization and the temporal TV regularization.

A reliable *a priori* estimate for the spatial sparsity level can be extracted from an anatomical MR image which is based on full cartesian sampling of the k-space and is in practice always taken as a part of the dynamic MRI measurement protocol but is usually used only for visualization purposes. In case an anatomical reference image is not acquired, the expected spatial sparsity could also be estimated from a static reconstruction of a long sequence of baseline of the dynamic data or from an anatomical atlas image.

An *a priori* estimate for the expected sparsity in the temporal regularization domain can be extracted from the dynamic MRI data. More specifically, the DC component of the k-space data gives the information about the integral intensity of the unknown image at each frame. This information can then be used to approximate the expected sparsity level of the time derivative of the images when the image changes are based on contrast changes instead of tissue movement. The approach leads to a simple two-dimensional search from a set of reconstructions over a grid of parameter values (α, β) .

The idea in the proposed method is basically a 2D extension of the S-curve method, which was originally proposed for the selection of regularization parameter in sparsity promoting regularization in [8] and later applied to parameter selection in (static) x-ray tomography in [9–11]. The S-curve method was also applied to spatial TV regularization parameter selection in DCE-MRI in [12].

Since the proposed 2D parameter search can require a large number of reconstructions

over a grid of values of (α, β) , we also consider a second method where the parameters α and β are selected separately by applying the S-curve method sequentially to first the temporal regularization parameter β and then the spatial regularization parameter α .

The proposed parameter selection approaches are evaluated using simulated and experimental DCE-MRI data from a rat brain study. The operation principle in DCE-MRI is to inject a bolus of gadolinium based contrast agent into the blood stream and acquire a time series of MRI data with a suitable T_1 -weighting to obtain a time series of 2D (or 3D) images which exhibit contrast changes induced by concentration changes of the contrast agent in the tissues. DCE-MRI is used for example in treatment monitoring of breast cancer [13, 14] and glioma [15], and to detect perfusion abnormalities in brain diseases [16, 17]. The proposed approach is demonstrated to lead to a highly feasible selection of regularization parameters.

2 Theory

2.1 Forward model

The discrete MRI measurement model for a single image with cartesian measurements is of the form

$$m = \mathcal{F}u + e, \quad (2)$$

where $m \in \mathbb{C}^M$ is a complex valued measurement vector, where M is the number of k-space measurement points, \mathcal{F} is the discrete Fourier transform, $u \in \mathbb{C}^N$ is a complex valued image, where N is the number of pixels in the image, and e models measurement noise. In the case of a non-cartesian k-space sampling trajectory, the Fourier transform can be approximated with the non-uniform fast Fourier transform (NUFFT) operation [18].

When NUFFT is used as the forward model, the measurement model can be written as

$$m = P\mathcal{F}Su + e, \quad (3)$$

where P is an interpolation matrix from cartesian k-space to the non-cartesian k-space trajectory and S is a scaling matrix. Hereafter we denote $A := P\mathcal{F}S$.

When considering dynamic MRI with complementary k-space sampling, where different (undersampled) trajectories of the k-space are measured at different time points, the forward model changes depending on the time point. The forward model can then be written as

$$m^t = P^t \mathcal{F} S^t u^t + e^t = A^t u^t + e^t, \quad (4)$$

where the integer valued superscript t denotes the time index of the measurement and image series, and m^t is the vector of k-space data for a single image in the time series, which is dependent on the selected data segmentation length.

2.2 Joint reconstruction formulation of the dynamic inverse problem

The CS based joint image reconstruction formulation we consider is

$$\hat{u} = \arg \min_{u=u^1, u^2, \dots, u^T} \left\{ \sum_{t=1}^T \left[\|A^t u^t - m^t\|_2^2 + \alpha \|\nabla_S u^t\|_1 \right] + \beta \|\nabla_T u\|_1 \right\}, \quad (5)$$

where T is the number of image frames in the problem, ∇_S is the discrete spatial gradient operator, α and β are regularization parameters for spatial and temporal regularizations respectively, and ∇_T is the discrete temporal gradient operator.

Here, we use the isotropic form of 2D spatial TV, where the total variation functional for a complex valued image u^t is defined as

$$\|\nabla_S u^t\|_1 = \sum_{k=1}^N \left((\text{Re}(D_x^k u^t))^2 + (\text{Re}(D_y^k u^t))^2 + (\text{Im}(D_x^k u^t))^2 + (\text{Im}(D_y^k u^t))^2 \right)^{1/2}, \quad (6)$$

where Re and Im denote taking the real and the imaginary parts of the complex valued image, k denotes the spatial index in the 2D images, and D_x^k and D_y^k are discrete forward differences in the horizontal and vertical image directions of the k 'th pixel defined as

$$D_x^k u^t = \begin{cases} -u_k^t + u_{k+n}^t, & \text{if } k \leq N - n \\ 0, & \text{otherwise} \end{cases}$$

$$D_y^k u^t = \begin{cases} -u_k^t + u_{k+1}^t, & \text{if } k \pmod{n} \neq 0 \\ 0, & \text{otherwise,} \end{cases}$$

where n is the number of rows and columns in the image that is assumed to be square.

Similarly, the temporal TV is defined by

$$\|\nabla_T u\|_1 = \sum_{t=1}^T \sum_{k=1}^N \sqrt{(\text{Re}(D_T^t u_k))^2 + (\text{Im}(D_T^t u_k))^2}, \quad (7)$$

where $u_k = u_k^1, \dots, u_k^T$ and D_T^t is the discrete forward difference in the temporal direction of the t 'th image defined as

$$D_T^t u_k = \begin{cases} -u_k^t + u_k^{t+1}, & \text{if } t \neq T \\ 0, & \text{otherwise.} \end{cases} \quad (8)$$

2.3 Selection of the regularization parameters

The S-curve was originally proposed for the selection of a regularization parameter in wavelet based sparsity promoting regularization in [8]. The idea in the S-curve method is to select the regularization parameter such that the reconstructed image has an *a priori* expected sparsity level in the regularization domain.

The CS formulation of the dynamic MRI problem in Eq. (5) includes two regularization parameters, α and β , making the parameter selection a two dimensional problem. Here, the idea of the S-curve method is extended to the selection of two regularization parameters, which we propose to select by finding the parameter pair $(\hat{\alpha}, \hat{\beta})$ that produces expected sparsity level in both the spatial and temporal regularization domains, with simultaneous or sequential selection of the parameters.

2.3.1 Selection of the *a priori* sparsity estimates

Assume that we have an *a priori* estimate

$$\hat{S}_S = \text{TV}_S(u^{\text{ref}}) := \|\nabla_S u^{\text{ref}}\|_1 \quad (9)$$

for the spatial total variation norm of a single unknown image u^t , obtained from a reference image u^{ref} . The reference image can be for example an anatomical image from fully sampled measurements, a conventional reconstruction of a long sequence of the baseline of the dynamic data or an anatomical atlas image.

Remark that in cases where the expected sparsity level \hat{S}_S is estimated from a reference image u^{ref} that has been acquired with different contrast parameters or comes from a different imaging modality, the reference image has to be scaled for calculation of \hat{S}_S such that it is compatible with the dynamic MRI data. This normalization of the reference image can be simply done, for example, by

$$u^{\text{ref}} \leftarrow \frac{\|m^1\|_2}{\|A^1 u^{\text{ref}}\|_2} u^{\text{ref}}, \quad (10)$$

where m^1 is the first baseline frame of dynamic MRI data and A^1 is the respective forward model.

When the temporal changes in the image are based on (mostly) unidirectional contrast changes, an estimate for the sparsity level \hat{S}_T of the temporal gradient can be obtained from the dynamic data using the zero frequency (DC) components of the k-space data. The sparsity estimate is based on the property that the DC component of the Fourier transform of a function f equals the total intensity of the image, i.e.

$$\hat{f}(0) = \int_{\Omega} f(r) dr.$$

Therefore, for the total intensity difference between two images (w, z) we have

$$\left| \int_{\Omega} w(r) dr - \int_{\Omega} z(r) dr \right| = |\hat{w}(0) - \hat{z}(0)|.$$

Thus, an estimate for the temporal total variation

$$\text{TV}_T(u) = \|\nabla_T u\|_1$$

of the unknown image sequence u can be obtained from the measurement data by

$$\hat{S}_T \approx \sum_{t=1}^{T-1} \left| m_{(k=0)}^{t+1} - m_{(k=0)}^t \right|, \quad (11)$$

where the subscript ($k = 0$) refers to one of the zero frequency components of the k-space data vector m^t .

Note that under ideal noiseless measurement data, the estimate \hat{S}_T would be a lower bound for the temporal TV of the image sequence. The difference between the zero-frequency k-space coefficients of two images would be equal to the time TV of the images when there is no noise or tissue movement and the contrast changes between the two images are completely unidirectional. When the contrast changes between the two images are of different signs in different parts of the target or the image changes are caused by motion, the difference of the zero-frequency k-space coefficients would underestimate the time TV between the images. In presence of measurement noise or forward model errors, the estimate (11) may also be larger than the true temporal TV of the unknown image sequence.

2.3.2 Simultaneous selection of the parameters (S-surface)

Given the estimates \hat{S}_T and \hat{S}_S of the *a priori* expected temporal and spatial sparsity, we select the regularization parameters (α, β) as follows:

- 1) Take a grid of regularization parameters α and β ranging on the interval $(0, \infty)$ such that

$$0 < \beta^{(1)} < \beta^{(2)} < \dots < \beta^{(P)} < \infty$$

and

$$0 < \alpha^{(1)} < \alpha^{(2)} < \dots < \alpha^{(L)} < \infty.$$

- 2) Compute the corresponding estimates $\hat{u}(\alpha^{(\ell)}, \beta^{(p)})$, $\ell = 1, \dots, L$, $p = 1, \dots, P$. The reconstructions $\hat{u}(\alpha^{(\ell)}, \beta^{(p)})$ are computed by

$$\hat{u} = \arg \min_{u=u^1, u^2, \dots, u^T} \left\{ \sum_{t=1}^T \left[\|A^t u^t - m^t\|_2^2 + \alpha^{(\ell)} \|\nabla_S u^t\|_1 \right] + \beta^{(p)} \|\nabla_T u\|_1 \right\}. \quad (12)$$

Here, it is crucial that $\beta^{(1)}$ is selected so small that the reconstructions have a larger time TV than the expected temporal sparsity level, and $\alpha^{(1)}$ is so small that the reconstructions have a larger spatial TV than the expected spatial sparsity level. Similarly, the values $\beta^{(P)}$ and $\alpha^{(L)}$ are selected so large that the problem becomes over-regularized and the respective TV values of the reconstructions are close to zero.

- 3) Compute the temporal TV of the image series $\text{TV}_T(\hat{u}(\alpha, \beta))$ and the spatial TV of one time frame of the image series $\text{TV}_S(\hat{u}^t(\alpha, \beta))$ for each grid point $(\alpha^{(\ell)}, \beta^{(p)})$.
- 4) Evaluate the value of the merit functional

$$\Psi(\alpha, \beta) = \frac{|\text{TV}_T(\hat{u}(\alpha, \beta)) - \hat{S}_T|}{2\hat{S}_T} + \frac{|\text{TV}_S(\hat{u}^t(\alpha, \beta)) - \hat{S}_S|}{2\hat{S}_S} \quad (13)$$

for each grid point.

- 5) Select the parameter pair $(\hat{\alpha}, \hat{\beta})$ which minimizes $\Psi(\alpha, \beta)$.

2.3.3 Sequential selection of the parameters (S-curve)

The two-dimensional selection of the parameters (α, β) in Section 2.3.2 requires computing a large number of reconstructions of the form of Eq. (5) over a 2D grid of regularization

parameter values, making it computationally expensive, especially in large 4D problems. Therefore, to alleviate the computational burden, we also consider an approach where we split the parameter search into two 1D problems.

We employ the S-curve first for the selection of the temporal regularization parameter β without any spatial regularization (i.e. $\alpha = 0$ in Eq. (5)), and then we employ the S-curve for the selection of the spatial regularization parameter α using the value of β found in the first step. We select the parameter β first since the reconstruction from undersampled measurements is more dependent on the temporal regularization than the spatial regularization.

Selection of β : Given the estimate \hat{S}_T of the *a priori* temporal sparsity level, we first select the temporal regularization parameter β using the S-curve as follows:

- 1) Take a sequence of regularization parameters β ranging on the interval $(0, \infty)$ such that

$$0 < \beta^{(1)} < \beta^{(2)} < \dots < \beta^{(P)} < \infty.$$

- 2) Compute the corresponding estimates $\hat{u}(\beta^{(1)}), \dots, \hat{u}(\beta^{(P)})$ according to

$$\hat{u}(\beta^{(p)}) = \arg \min_{u=u^1, u^2, \dots, u^T} \left\{ \sum_{t=1}^T \|A^t u^t - m^t\|^2 + \beta^{(p)} \|\nabla_T u\|_1 \right\}. \quad (14)$$

Here too, $\beta^{(1)}$ has to be so small that the problem is under-regularized and the corresponding reconstruction $\hat{u}(\beta^{(1)})$ is a noisy image sequence with a time TV larger than \hat{S}_T and $\beta^{(P)}$ is so large that the problem is over-regularized and the time TV of the reconstruction is close to zero.

- 3) Compute the time TV of the recovered estimates $\hat{u}(\beta^{(p)})$, $p = 1, \dots, P$.
- 4) Fit a smooth interpolation curve to the data $\{\beta^{(p)}, \text{TV}_T(\hat{u}(\beta^{(p)}))\}$, $p = 1, \dots, P$ and use the interpolated sparsity curve to find the value $\hat{\beta}$ for which $\text{TV}_T(\hat{\beta}) = \hat{S}_T$.

Selection of α : Given the value $\hat{\beta}$ and the *a priori* expected spatial sparsity level \hat{S}_S , the spatial regularization parameter α is selected according to the following procedure:

- 1) Take a sequence of regularization parameters α ranging on the interval $(0, \infty)$ such that

$$0 < \alpha^{(1)} < \alpha^{(2)} < \dots < \alpha^{(L)} < \infty.$$

2) Compute the corresponding estimates $\hat{u}(\alpha^{(1)}), \dots, \hat{u}(\alpha^{(L)})$ by

$$\hat{u}(\alpha^{(\ell)}, \hat{\beta}) = \arg \min_{u=u^1, u^2, \dots, u^T} \left\{ \sum_{t=1}^T \left[\|A^t u^t - m^t\|_2^2 + \alpha^{(\ell)} \|\nabla_S u^t\|_1 \right] + \hat{\beta} \|\nabla_{T u}\|_1 \right\}. \quad (15)$$

Again, $\alpha^{(1)}$ needs to be so small that a frame in the reconstruction $\hat{u}(\alpha^{(1)})$ results in a spatial TV larger than \hat{S}_S and $\alpha^{(L)}$ needs to be so large that the spatial TV of a frame $\hat{u}(\alpha^{(L)})$ is very small.

3) Compute the spatial TV of a frame of the recovered estimates $\hat{u}(\alpha^{(\ell)}, \hat{\beta})$, $\ell = 1, \dots, L$, i.e. $\text{TV}_S(\hat{u}^t(\alpha^{(\ell)}, \hat{\beta}))$.

4) Fit a smooth interpolation curve to the data $\{\alpha^{(\ell)}, \text{TV}_S(\hat{u}^t(\alpha^{(\ell)}, \hat{\beta}))\}$, $\ell = 1, \dots, L$, and use the interpolated sparsity curve to find the value $\hat{\alpha}$ for which $\text{TV}_S(\hat{\alpha}, \hat{\beta}) = \hat{S}_S$.

The final reconstruction for analysis and diagnostic tasks can then be computed using the parameter pair $(\hat{\alpha}, \hat{\beta})$.

3 Methods

3.1 Simulated test case

A simulated test case modelling DCE-MRI of a glioma in a rat brain was created. The rat brain phantom is based on the rat brain atlas [19], and the phantom was scaled to a size of 128x128. The rat brain image was divided into three subdomains of different signal behaviour: simulated vascular region (highlighted with blue and labelled '1' in Fig. 1), simulated tumour region (highlighted with red and labelled '2' in Fig. 1) and the rest of the brain tissue. The vascular signal region corresponds to the location of the superior sagittal sinus which can be used as a proxy for estimating the arterial input function (AIF) in DCE-MRI of the brain [20]. The AIF is used in the estimation of pharmacokinetic parameters in DCE-MRI [21], and the vascular region is thus of special interest.

A time series of 2800 ground truth images was simulated by multiplying the signal of each pixel with a signal template of the corresponding region and adding that to the baseline value of the pixels. The signal templates were based on an experimental DCE-MRI measurement, which is described briefly in Sect. 3.2 and also in [22, 23], from which

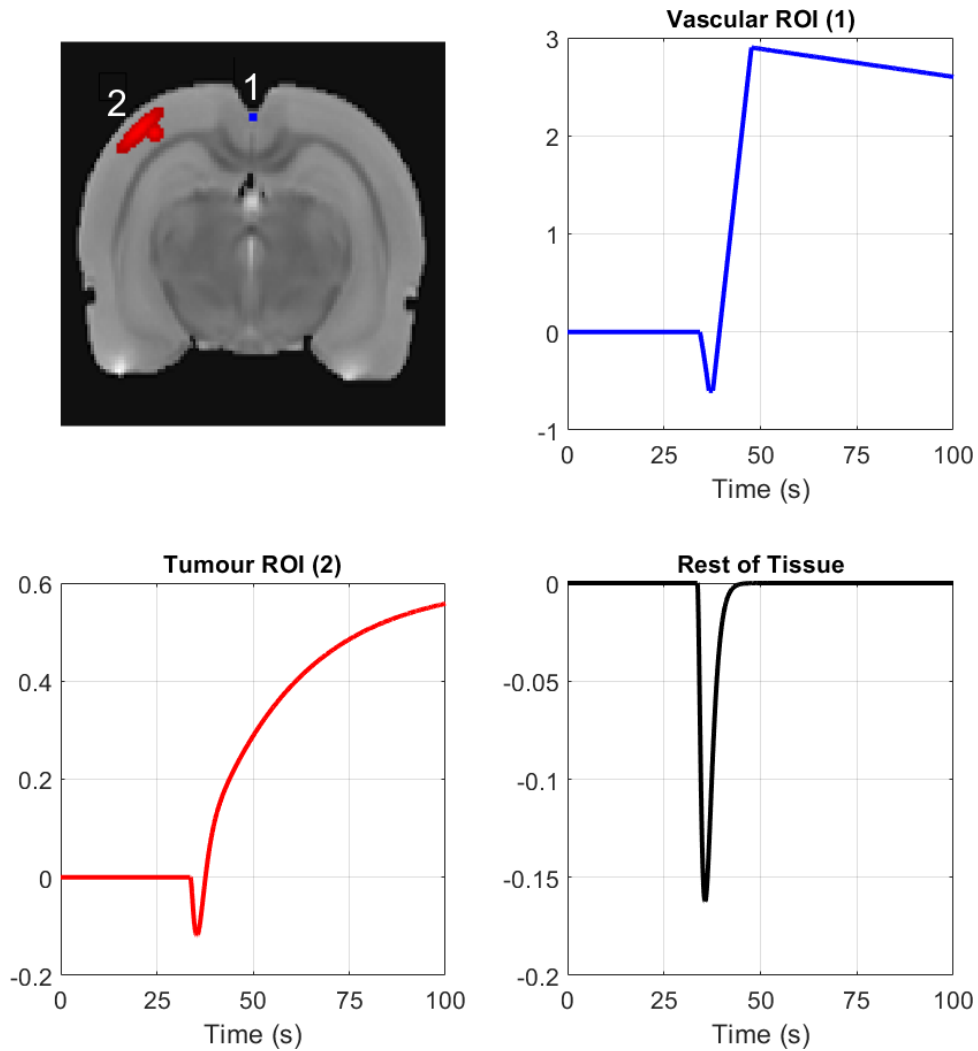


Figure 1: Vascular and tumour regions and the three template signals used in the simulation. Top left: The simulated image with vascular ROI marked in blue and labelled '1', and tumour ROI marked in red and labelled '2'. Top right: Simulated vascular ROI signal template. Bottom left: Simulated tumour ROI signal template. Bottom right: Simulated signal template in the rest of the tissue. Each image pixel was multiplied with the corresponding template and the result was added to the image to create the simulated time series.

the three different ROIs were identified. Fig. 1 shows the signal templates for each of the different tissue regions. The same simulated test case has been used previously in [12, 22].

The simulated test case was carried out using a k-space trajectory which combines the golden angle (GA) [24] and the concentric squares sampling strategies [25, 26].

One spoke of k-space data was simulated for each of the simulated images, leading to a dynamic experiment with 2800 spokes of k-space data. The time scale of the simulated signal dynamics was set to be similar to the in vivo measurements where the repetition time of the GA measurements was 38.5 ms. Complex gaussian noise at 5% of the mean of the absolute values of the signal was added to the simulated k-space signal.

3.1.1 Error metric for the simulation

Root mean square error (RMSE) values were calculated for the three regions of interest: 1) vascular region, 2) tumour region and 3) the rest of the image. For the calculation of the RMSE, the reconstructed signals of each pixel were linearly interpolated in the temporal direction to match with the temporal resolution of the ground truth phantom (i.e., segment length of one spoke). After the interpolation, RMSE to the ground truth phantom was calculated for all regions separately. After the RMSEs for the three ROIs were computed, a joint RMSE was computed by taking the norm of the separate RMSEs. This was done to weigh the ROIs with a small support (vascular, tumour) appropriately in the error metric. The error metric was selected independent of the parameter selection, and the same metric was used in [12, 22]. The error metric is described in more detail in [22].

3.2 In vivo measurements from a rat glioma model

All animal experiments were approved by the Animal Health Welfare and Ethics Committee of University of Eastern Finland. Experimental DCE-MRI data was acquired from a female Wistar rat with a glioma model [27]. Imaging was performed 10 days post-implantation of the glioma cells into the rat brain. During the experiments, the animal was anesthetized and kept in fixed position in a holder which was inserted into the magnet. A needle was placed into the tail vein of the animal for the injection of the contrast agent.

The DCE data were collected using a 9.4 T horizontal magnet interfaced to an Agilent imaging console and a volume coil transmit/quadrature surface coil receive pair (Rapid Biomed, Rimpar, Germany). The data were collected with a radial golden angle sampling using a gradient-echo based radial pulse sequence with repetition time 38.5 ms, echo time 9 ms, flip angle 30 degrees, field-of view 32 mm x 32 mm, slice thickness 1.5 mm and number of points in each spoke 128. 610 spokes were collected in sequential order, after which the next spoke would differ by less than 0.1 degrees from the first spoke, so to simplify the experimental sequence, the cycle of 610 spokes was repeated. The cycle was repeated for a total of 25 times, leading to an overall measurement sequence of 15250 spokes of data for a total measurement duration of nearly 10 minutes. Measurement time for a cycle of 610 spokes was $610 \cdot 38.5 \text{ ms} = 23.46 \text{ s}$. Gadovist (1 mmol/kg) was injected i.v. one minute after the beginning of the dynamic scan over a period of 3 s. In the experimental data results section, 7320 spokes of data from the beginning of the measurements were used for testing the proposed parameter selection approach.

Anatomical images were also acquired from the same slice before and after the dynamical experiment using a gradient-echo pulse sequence with otherwise similar parameters as in the dynamic sequence but using a full Cartesian sampling of 128x128 points of k-space data. The full data anatomical images with spatial regularization from before and after the experiment are shown as reference for the dynamical reconstructions with undersampled data in Fig. 2.

The dynamical experiment also served as a basis for creating the signal templates shown in Fig. 1 for the simulated test case. For the simulation, three regions were identified from the in vivo reconstructions: vascular region (superior sagittal sinus), glioma region, and the rest of the brain tissue.

3.3 Computation

The Chambolle-Pock primal-dual algorithm [28, 29] was used to solve the minimization problem of Eq. (5). The ratio of the primal and dual step sizes was varied according to the regularization coefficients such that the primal step size was smaller (and accordingly the dual step size was larger) for larger regularization parameters. Asymmetrical primal and dual step sizes in the algorithm have been shown to lead to faster convergence in some cases in both linear [30] and non-linear [31] problems, and this was observed here

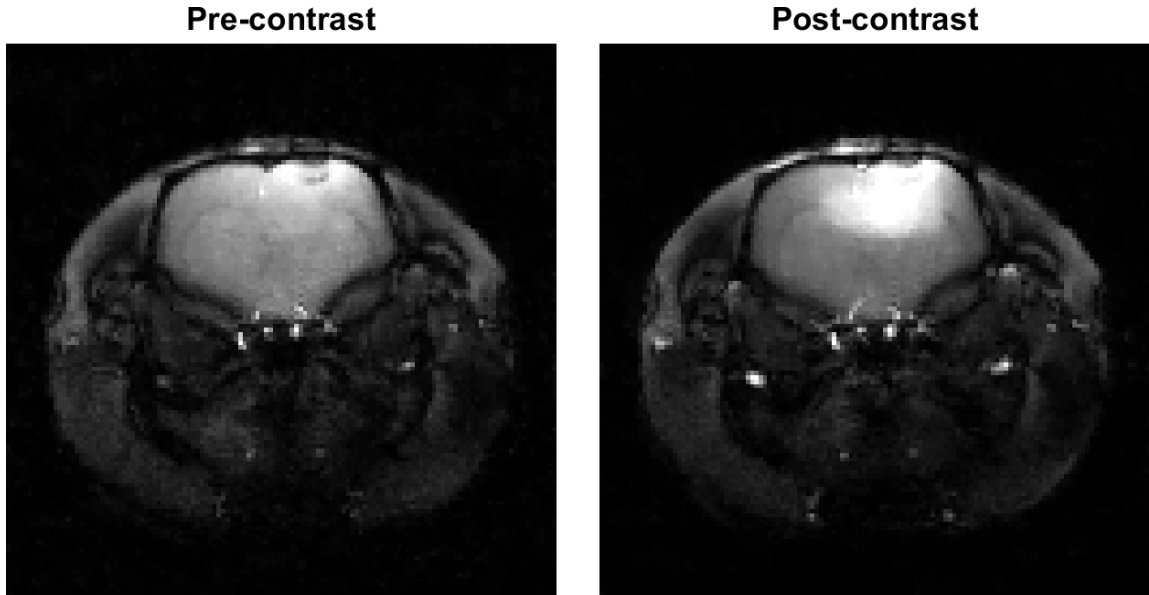


Figure 2: Cartesian gradient-echo pulse sequence full data reconstructions with spatial regularization from before and after contrast injection used as reference. The two images have the same adjusted color scale.

as well. The operator norms of the forward problem, and the spatial and temporal total variation terms were all scaled to 1.

4 Results

4.1 Simulated data

For the simulation, we use the parameter pair and the reconstruction that yields the lowest joint RMSE as references of the best possible parameter pair and reconstruction. We refer to this parameter selection method as MinRMSE and compare the S-surface and S-curve methods to the MinRMSE. The regularization parameters selected with the different methods are shown in Table 1.

Figs. 3 - 5 show the results using the simulated rat brain DCE data. Fig. 3 shows single frames of the reconstructions after contrast agent injection as well as single pixel signals from the tumour and vascular areas as well as healthy tissue on the right side of the cortex. The reconstructions appear similar in quality and there are only slight differences in the single pixel signals. Fig. 3 also shows the RMS errors of the three different regions.

Table 1: The spatial ($\hat{\alpha}$) and temporal ($\hat{\beta}$) regularization parameters for the simulated test case obtained with the S-surface and S-curve methods and the MinRMSE parameters used as reference.

	MinRMSE	S-surface	S-curve
$\hat{\alpha}$	0.0001	0.00032	0.00021
$\hat{\beta}$	0.0032	0.0032	0.0064

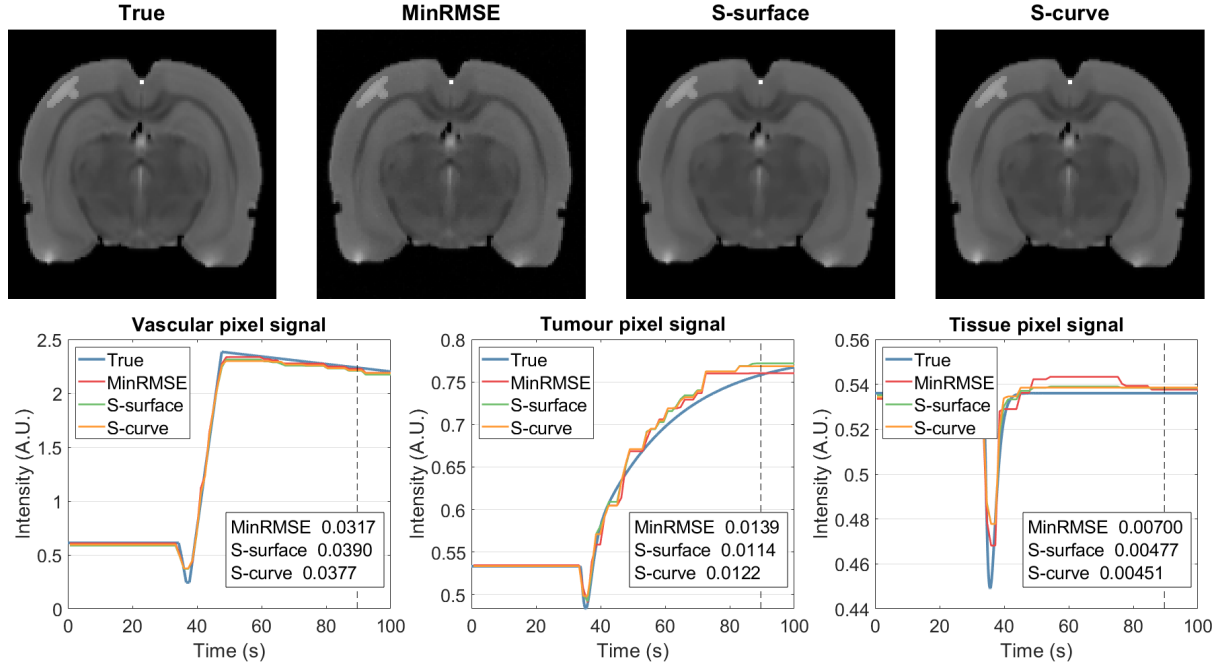


Figure 3: Top row: Single frame images of the simulated true target and reconstructions at $t \approx 90$ s (marked below with a dashed line) with parameters chosen with different methods; minimum joint RMSE (MinRMSE), simultaneous parameter selection according to joint sparsity (S-surface) and sequential parameter selection according to sparsity (S-curve). Bottom row: Single pixel signals from the vascular and tumour areas as well as healthy tissue from the right side of the cortex with the different methods compared to the phantom and RMS errors of the corresponding regions.

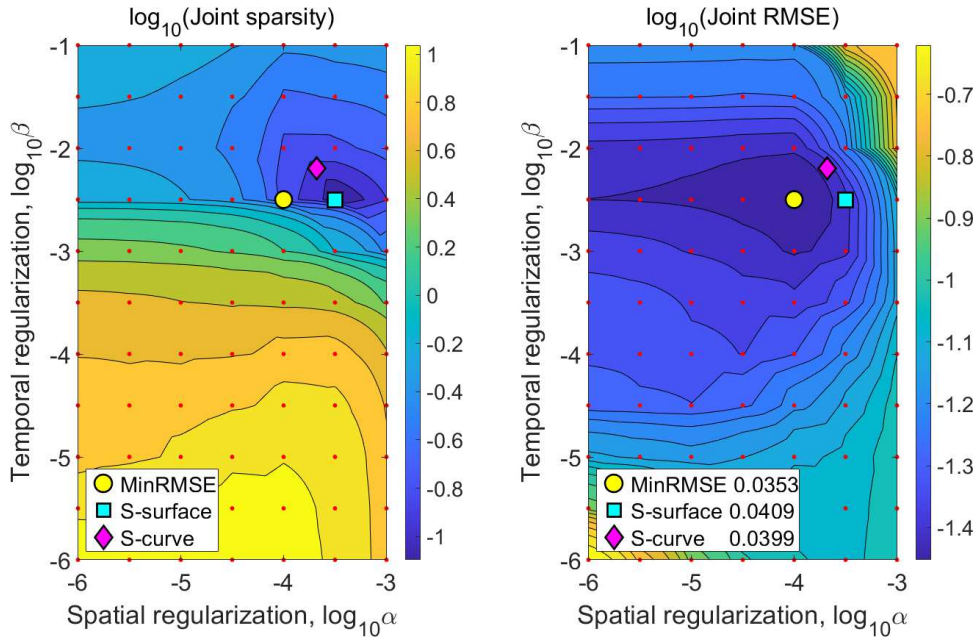


Figure 4: Left: Joint sparsity contour with the parameters of the three different reconstructions marked. Right: Joint RMSE contour with the same parameter pairs marked, and the RMSE values corresponding to the three reconstructions, which also show that the reconstructions obtained with the S-surface and S-curve methods are close to the optimal (MinRMSE). The red dots mark the tested parameter pairs. The obtained parameter pairs $(\hat{\alpha}, \hat{\beta})$ were MinRMSE = (0.0001, 0.0032), S-surface = (0.00032, 0.0032), S-curve = (0.00021, 0.0064).

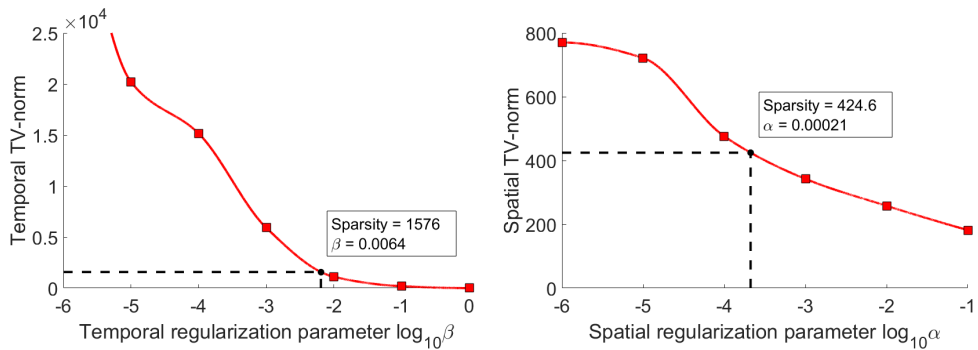


Figure 5: The temporal and spatial S-curves, and the sparsity levels and regularization parameters corresponding to the *a priori* sparsity estimates of the simulated reconstructions. The red squares mark the 1D grid of regularization parameters.

Fig. 4 shows the joint sparsity and joint RMSE contours of the reconstructions calculated on a wide grid of the spatial and temporal regularization parameters. Fig. 4 also shows the joint RMSE values of the reconstructions with the parameters chosen with the three different methods. The joint RMSE values for the S-surface and S-curve reconstructions are close to those of the optimal reconstruction (MinRMSE), and the regularization parameters obtained with the S-surface and S-curve methods are close to the MinRMSE parameters.

Fig. 5 shows both the temporal and spatial S-curves as well as the sparsity levels and parameter values taken from the interpolated curve for the sequential parameter selection method. The reference temporal sparsity was obtained by taking the spoke closest to vertical from each segment of 34 spokes, and calculating the total intensity changes using the DC signal of those spokes. This selection was done due to the DC signal of the real measurements having some dependence on the angle of the measurement spoke. The reference spatial sparsity level used was the spatial total variation of the first frame of the ground truth phantom. Note here, that since the temporal regularization parameter was first selected, the selection of the spatial regularization parameter value is not as sensitive as the temporal regularization parameter selection.

4.2 Experimental data

Figs. 6 - 7 show the results for the experimental data. Fig. 6 shows the cartesian reference reconstruction with spatial regularization from before contrast agent injection and single frame images from the dynamic reconstructions using parameters obtained with the S-surface and S-curve methods from after the contrast agent injection. The reference image is the same as in Fig. 2. Fig. 6 also contains single pixel signals from the tumour and vascular regions. The reconstructions are visually similar and the single pixel signals show little difference with the S-curve reconstruction having slightly smaller signal changes.

Fig. 7 shows the joint sparsity grid of reconstructions with a large grid of spatial and temporal regularization parameters where the S-surface and S-curve parameter pairs are marked. The figure also shows the temporal and spatial S-curves with the parameters obtained with the S-curve method. The parameters obtained with the two methods are almost the same, namely, the S-curve parameters are $\alpha = 0.00034$ and $\beta = 0.0097$, and the S-surface parameters are $\alpha = 0.00032$ and $\beta = 0.01$.

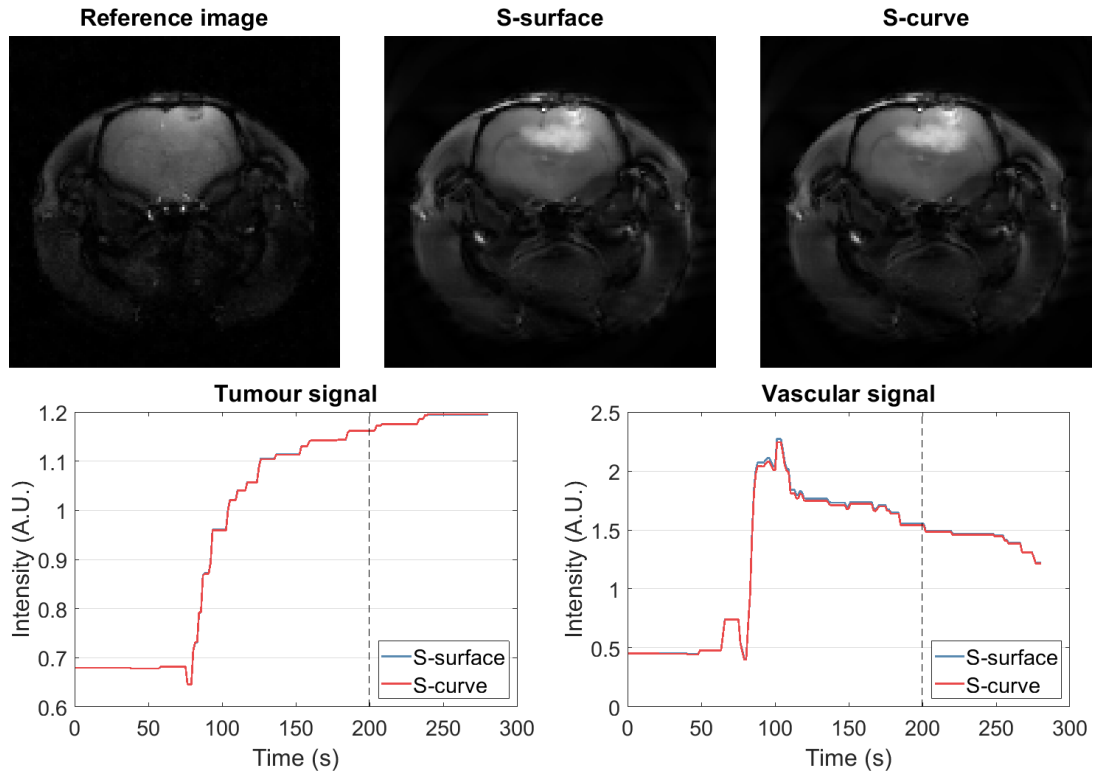


Figure 6: Top row: Single frame images of the cartesian reference image with spatial regularization from before contrast agent injection and the reconstructions of the experimental data at $t \approx 200$ s (marked below with a dashed line) with parameters chosen with the S-surface and S-curve methods. Bottom row: Single pixel signals from the tumour and vascular areas with the two different methods.

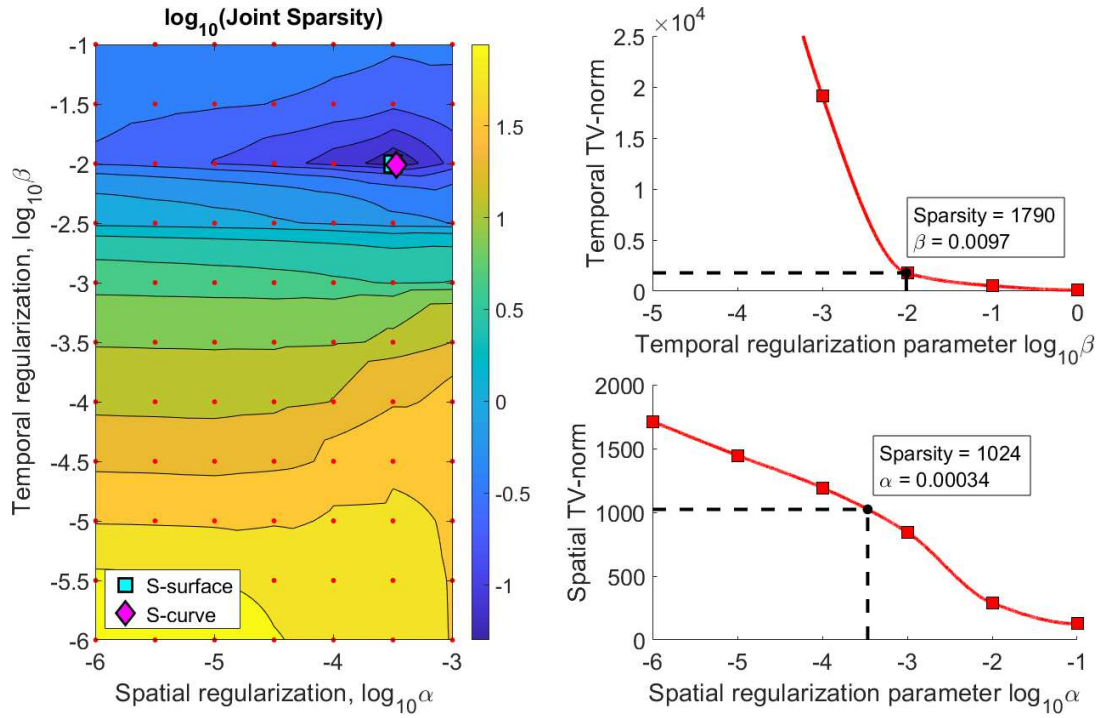


Figure 7: Left: Joint sparsity contour of the experimental reconstructions with different parameter pairs and the parameter pairs selected with the S-surface and S-curve methods. Red dots mark the tested parameter pairs. Right: The temporal and spatial S-curves and the sparsity and parameter values corresponding to the *a priori* sparsity estimates of the experimental reconstructions. The obtained parameter pairs $(\hat{\alpha}, \hat{\beta})$ were S-surface = $(0.00032, 0.01)$, S-curve = $(0.00034, 0.0097)$.

5 Discussion

Compressed sensing based models for dynamic MRI problems usually include regularization for sparsity in both the spatial and temporal domain. Therefore these models typically include two regularization parameters, one for the spatial and one for the temporal regularization, that the user has to select. Typically, the selection of both of the parameters is carried out manually based on visual assessment of the reconstructed images.

In this work, we investigated a two-dimensional parameter selection problem and proposed two parameter selection methods using *a priori* image sparsity estimates obtained from the k-space data for temporal sparsity and from a reference image for spatial sparsity. The evaluations of the methods were carried out using both simulated and experimental golden angle DCE-MRI data. The two parameter selection methods proposed were the S-surface and S-curve methods. In the simulated test case, the parameter selection methods were also compared with a parameter pair that gives the smallest joint RMS reconstruction error with respect to the true target images.

Both parameter estimation methods produced a parameter pair that is close to the parameter pair with the minimum joint RMSE in the simulated test case, and the RMSE reconstruction errors with these parameter selections were only slightly larger than the minimum RMSE. In the experimental case there is no minimum RMSE solution or other known optimal reference solution available, but the parameter pairs obtained with the proposed methods are close to a manually selected parameter pair. The visual reconstructions and signal dynamics were also similar in the reconstructions obtained with the different methods.

As is seen from Fig. 4, the parameter pairs obtained with the S-surface and S-curve methods have slightly higher spatial regularization values compared with the parameter pair that is optimal in the minimum joint RMSE sense. The temporal regularization parameter selected with the S-curve method is close to the MinRMSE parameter value, and the S-surface temporal regularization value is exactly the same as in the MinRMSE regularization parameter pair.

While the S-surface method is based on a 2D search which requires reconstructions over a grid of $P \times L$ parameter pairs (α, β) , the S-curve method is based on two 1D

searches, and therefore it needs only $P + L$ reconstructions making it computationally more efficient than the S-surface method. This suggests that the S-curve based selection could be a more favourable choice, especially in large scale 4D problems, as the methods produced similar parameter selection and reconstruction accuracy.

As the expected temporal sparsity level \hat{S}_T for the selection of the temporal regularization parameter is estimated from differences of the zero frequency components of the measured k-space data between consecutive time steps, the estimate provides an approximation for the temporal total variation of the unknown image series. In the simulated test case, the discrepancy between the true time TV of the ground truth images and the estimate \hat{S}_T obtained from the noisy k-space data using Eq. (11) was approximately 22% due to the high noise level in the simulated k-space data. Despite this discrepancy, the proposed parameter selections yielded highly feasible regularization parameters. However, we remark that in cases where the images between consecutive time steps exhibit changes due to motion or large opposite signed contrast changes that would lead to only small changes in the zero frequency coefficients, the data based sparsity estimate could be clearly smaller than the actual time TV, potentially leading to a less optimal parameter choice.

6 Conclusions

In this work, we proposed to use two sparsity based methods based on *a priori* sparsity estimates for the automatic selection of the regularization parameters for the TV regularized CS problem. The S-surface method selects the regularization parameters based on the expected sparsity of unknown images in the two domains of regularization simultaneously. We also adopted a faster method called the S-curve, where the regularization parameters were selected one at a time, which was shown to produce similar reconstruction accuracy and parameter selection. The S-curve method requires the computation of fewer reconstructions making it computationally more efficient.

Both of the approaches were demonstrated to lead to a highly feasible choice of the temporal and spatial regularization parameters in both the simulated and the experimental DCE-MRI experiment of a rat brain.

Acknowledgements

This work was supported by the Academy of Finland (Project 312343, Finnish Centre of Excellence in Inverse Modelling and Imaging, 2018–2025), the Jane and Aatos Erkko Foundation and the Väisälä Fund.

References

- ¹J. I. Jackson, C. H. Meyer, D. G. Nishimura, and A. Macovski, “Selection of a convolution function for Fourier inversion using gridding (computerised tomography application)”, *IEEE Trans Med Imaging* **10**, 473–478 (1991).
- ²E. J. Candes, J. Romberg, and T. Tao, “Robust uncertainty principles: exact signal reconstruction from highly incomplete frequency information”, *IEEE Trans Inf Theory* **52**, 489–509 (2006).
- ³D. L. Donoho, “Compressed sensing”, *IEEE Trans Inf Theory* **52**, 1289–1306 (2006).
- ⁴M. Lustig, D. Donoho, and J. M. Pauly, “Sparse MRI: the application of compressed sensing for rapid MR imaging”, *Magn Reson Med* **58**, 1182–1195 (2007).
- ⁵O. N. Jaspan, R. Fleysheer, and M. L. Lipton, “Compressed sensing MRI: a review of the clinical literature”, *Br J Radiol* **88**, 1–12 (2015).
- ⁶R. Acar and C. R. Vogel, “Analysis of bounded variation penalty methods for ill-posed problems”, *Inverse Prob* **10**, 1217–1229 (1994).
- ⁷G. Adluru, C. McGann, P. Speier, E. G. Kholmovski, A. Shaaban, and E. V. R. Dibella, “Acquisition and reconstruction of undersampled radial data for myocardial perfusion magnetic resonance imaging”, *J Magn Reson Imaging* **29**, 466–473 (2009).
- ⁸V. Kolehmainen, M. Lassas, K. Niinimäki, and S. Siltanen, “Sparsity-promoting Bayesian inversion”, *Inverse Prob* **28**, 025005 (2012).
- ⁹K. Hämmäläinen, A. Kallonen, V. Kolehmainen, M. Lassas, K. Niinimäki, and S. Siltanen, “Sparse tomography”, *SIAM J Comp* **35**, B644–B665 (2013).
- ¹⁰K. Niinimäki, “Computational optimization methods for large-scale inverse problems”, PhD thesis (University of Eastern Finland, 2013).

- ¹¹K. Niinimäki, M. Lassas, K. Hämäläinen, et al., “Multiresolution parameter choice method for total variation regularised tomography”, *SIAM J Imaging Sci* **9**, 938–974 (2016).
- ¹²K. Niinimäki, M. Hanhela, and V. Kolehmainen, “Parameter selection in dynamic contrast-enhanced magnetic resonance tomography”, <https://arxiv.org/abs/2002.09129>. To appear in *Springer Proc Math Stat.*, 2019.
- ¹³L. Martincich, F. Montemurro, G. D. Rosa, et al., “Monitoring response to primary chemotherapy in breast cancer using dynamic contrast-enhanced magnetic resonance imaging”, *Breast Cancer Res Treat* **83**, 67–76 (2004).
- ¹⁴M. Pickles, M. Lowry, D. Manton, P. Gibbs, and L. Turnbull, “Role of dynamic contrast enhanced MRI in monitoring early response of locally advanced breast cancer to neoadjuvant chemotherapy”, *Breast Cancer Res Treat* **91**, 1–10 (2005).
- ¹⁵F. Piludu, S. Marzi, A. Pace, et al., “Early biomarkers from dynamic contrast-enhanced magnetic resonance imaging to predict the response to antiangiogenic therapy in high-grade gliomas”, *Neuroradiology* **57**, 1269–1280 (2015).
- ¹⁶Z. Merali, K. Huang, D. Mikulis, F. Silver, and A. Kassner, “Evolution of blood-brain-barrier permeability after acute ischemic stroke”, *PLoS One* **12**, 1–11 (2017).
- ¹⁷K. Villringer, B. E. S. Cuesta, A.-C. Ostwaldt, et al., “DCE-MRI blood–brain barrier assessment in acute ischemic stroke”, *Neurology* **88**, 433–440 (2017).
- ¹⁸J. A. Fessler and B. P. Sutton, “Nonuniform fast Fourier transforms using min-max interpolation”, *IEEE Trans Signal Process* **51**, 560–574 (2003).
- ¹⁹P. A. Valdés-Hernández, A. Sumiyoshi, H. Nonaka, et al., “An in vivo MRI template set for morphometry, tissue segmentation, and fMRI localization in rats”, *Front Neuroinf* **5**, 26 (2011).
- ²⁰C. Lavini and J. J. Verhoeff, “Reproducibility of the gadolinium concentration measurements and of the fitting parameters of the vascular input function in the superior sagittal sinus in a patient population”, *Magn Reson Imaging* **28**, 1420–1430 (2010).
- ²¹P. S. Tofts, G. Brix, D. L. Buckley, et al., “Estimating kinetic parameters from dynamic contrast-enhanced T1-weighted MRI of a diffusable tracer: standardized quantities and symbols”, *J Magn Reson* **10**, 223–232 (1999).

- ²²M. Hanhela, M. Kettunen, O. Gröhn, M. Vauhkonen, and V. Kolehmainen, “Temporal regularization methods in DCE-MRI”, <https://arxiv.org/abs/2003.08652>. Submitted to *Journal of Mathematical Imaging and Vision.*, 2019.
- ²³J. Rasch, V. Kolehmainen, R. Nivajärvi, et al., “Dynamic MRI reconstruction from undersampled data with an anatomical prescan”, *Inverse Prob* **34**, 074001 (2018).
- ²⁴S. Winkelmann, T. Schaeffter, T. Koehler, H. Eggers, and O. Doessel, “An optimal radial profile order based on the golden ratio for time-resolved MRI”, *IEEE Trans Med Imaging* **26**, 68–76 (2007).
- ²⁵A. Averbuch, R. R. Coifman, D. L. Donoho, M. Elad, and M. Israeli, “Fast and accurate Polar Fourier transform”, *Appl Comput Harmon Anal* **21**, 145–167 (2006).
- ²⁶Y. Yang, F. Liu, M. Li, et al., “Pseudo-polar Fourier transform based compressed sensing MRI”, *IEEE Trans Biomed Eng* **64**, 816–825 (2016).
- ²⁷R. Nivajärvi, V. Olsson, V. Hyppönen, et al., “Detection of lentiviral suicide gene therapy in C6 rat glioma using hyperpolarised [1-13C]pyruvate”, *NMR Biomed* (2020) 10.1002/nbm.4250.
- ²⁸A. Chambolle and T. Pock, “A first-order primal-dual algorithm for convex problems with applications to imaging”, *J Math Imaging Vision* **40**, 120–145 (2011).
- ²⁹E. Y. Sidky, J. H. Jørgensen, and X. Pan, “Convex optimization problem prototyping for image reconstruction in computed tomography with the Chambolle-Pock algorithm”, *Phys Med Biol* **57**, 3065 (2012).
- ³⁰T. Pock and A. Chambolle, “Diagonal preconditioning for first order primal-dual algorithms in convex optimization”, in *Proc ieee int conf comput vis* (2011), pp. 1762–1769.
- ³¹T. Valkonen, “A primal–dual hybrid gradient method for nonlinear operators with applications to MRI”, *Inverse Prob* **30**, 55012 (2014).